Controls on phytolith stability upon exposure in paddy soils

Nicolai Koebernick [a,b,*], Robert Mikutta [a], Klaus Kaiser [a], Anika Klotzbücher [a], Anh T. Q. Nguyen [c], Minh N. Nguyen [c], Thimo Klotzbücher [a]

[a] Soil Science and Soil Protection, Martin Luther University Halle-Wittenberg, Von-Seckendorff-Platz 3, 06120 Halle (Saale), Germany
[b] School of Life Sciences, Root-Soil Interaction, Technical University of Munich, Emil-Ramann-Str. 4, 85354 Freising, Germany
[c] Faculty of Environmental Sciences, University of Science, Vietnam National University, Hanoi (VNU), 334 NguyenTrai, Thanh Xuan, Hanoi, Viet Nam

ARTICLE INFO

ABSTRACT

Phytoliths are an important component in the cycling of silicon (Si) in rice cultivation, yet little is known about their medium to long-term stability. While it is commonly accepted that phytolith solubility in soil decreases with time, the mechanisms that cause this decrease remain unclear. Most studies on phytolith aging to date have been conducted under laboratory conditions and field studies are rare. Here, we present a comprehensive field study of phytolith aging in paddy and non-paddy fields in the Philippines and Vietnam. Phytoliths extracted from rice straw were placed in mesh bags and exposed to ambient soil conditions for up to 550 days. Following exposure, total mass loss and changes in physical (particle size, specific surface area, ζ potential) and chemical (surface chemical composition by acid digestion and X-ray photoelectron spectroscopy) properties as well as dissolution kinetics (56 days in 0.1 M $CaCl_2$ at pH 6.5) were determined. Phytolith dissolution in the field was rapid (up to 30 % mass loss) and three times faster in paddy than in non-paddy soils. Differences in phytolith properties were unexpectedly little between paddy and non-paddy soils. Laboratory and field-derived dissolution rates decreased with exposure time but were one order of magnitude lower in the field. While laboratory dissolution rates were negatively related to surface Al contents this was not observed for field-exposed phytoliths. Our findings suggest that under natural field conditions, phytolith dissolution is overwhelmingly governed by water regime, while the influence of protective surface coatings is only minor. We conclude that reliable estimates of phytolith dissolution can be best obtained in field experiments.

1. Introduction

Silicon (Si) is a beneficial element for many plants, enhancing the resistance against herbivory, pathogens, and abiotic stress such as drought and mechanical strain (Guntzer et al., 2012). Rice (*Oryza sativa* L.) is one of the most effective Si-accumulating plants; the Si content of rice plants can attain up to 10 % of dry matter. Silicon is taken up from soil solution as silicic acid ($H_4SiO_4^0$) and transported to plant tissues where it precipitates to form amorphous silica ($SiO_2 \times n\ H_2O$, opal A) bodies, called phytoliths (Parr and Sullivan, 2005; Piperno, 2006). These phytoliths are returned to soil with litter and serve as an important source of plant-available Si because their solubility within common soil pH range is 1–4 orders of magnitude greater than that of most silicate minerals (Fraysse et al., 2009). Especially in older soils, where the pool of weatherable minerals is depleted, phytoliths become the dominant source of plant-available Si (de Tombeur et al., 2020). In agricultural

environments, the regular export of Si bound in aboveground biomass disrupts the biological feedback loop and causes the depletion of plant-available Si (Vandevenne et al., 2012). Desplanques et al. (2006) have estimated that agricultural Si exports from a paddy soil in Camargue, France, can exhaust plant-available Si stocks in as little as five years. As a result, some rice cultivation systems become Si limited, which could contribute to yield decline (Savant et al., 1997). Silicon limitation may in fact be widespread and has been reported for various rice producing regions, including Vietnam, Sub-Saharan Africa, and the southern USA (Klotzbücher et al., 2016; Kraska and Breitenbeck, 2010; Tsujimoto et al., 2014). Reincorporation of rice straw into paddy fields could be a cost-effective way to mitigate the loss of plant-available Si (Klotzbücher et al., 2016; Marxen et al., 2016; Savant et al., 1997; Yang et al., 2020). Straw decomposition experiments in mesocosms showed that Si release from fresh rice straw happened fast and the released Si was immediately plant-available, as rice plants with straw addition showed increased Si

uptake (Marxen et al., 2016). However, Si release rates decreased with time, suggesting that phytoliths stabilize over time in soil. Other studies showed that "old" phytoliths extracted from soil had smaller dissolution rates than "fresh" phytoliths (Cabanes and Shahack-Gross, 2015; Cabanes et al., 2011; Fraysse et al., 2006; Liu et al., 2023). This is commonly explained by partial phytolith dissolution, where the most labile fraction of a phytolith assemblage dissolves fast, leaving behind a more resistant fraction (Alexandre et al., 1997; Blecker et al., 2006).

The factors that render some phytoliths less soluble over time are not fully understood. Fraysse et al. (2006) found that the differences in solubility between "fresh" and "soil" phytoliths was explained by the higher specific surface area (SSA) of "fresh" phytoliths. In a later study however, Fraysse et al. (2009) found that despite differences in SSA among the phytoliths of four plant species, their solubility was similar. They also showed that the SSA of phytoliths did not decrease during the initial 1–1.5 months of dissolution; for two of the analyzed species SSA even increased (Fraysse et al., 2009). Cabanes and Shahack-Gross (2015) showed that the solubility of phytolith assemblages was mainly explained by their surface area to bulk ratios rather than SSA. Liu et al. (2023) showed that partial dissolution led to the disappearance of fine surface structures, and a narrowing of the particle size distribution due to the loss of small particles. Aside from phytolith morphology, the chemical composition of phytoliths influences their solubility. Bartoli and Wilding (1980) and Bartoli (1985) suggested that surface-adsorbed aluminum (Al) decreases the solubility of phytoliths. Correspondingly, Nguyen et al. (2014) found that phytolith solubility dropped strongly in presence of dissolved Al^{3+}, likely due to sorption on deprotonated SiO^{-} sites. Aluminum can also be incorporated into the structure of silica, which might explain why Fraysse et al. (2009) found no correlation between phytolith Al content and dissolution rates. Phytoliths may likewise be coated by iron (Fe) oxide phases (Calegari et al., 2013),

particularly in redox-active environments such as paddy soils. Recently, we showed that accumulation of Fe oxides after exposure to soil solutions under oscillating redox conditions decreased the dissolution rates of phytoliths (Koebernick et al., 2022). Coatings of Fe and Al oxides could also promote micro-aggregation of phytoliths due to the opposing surface charge at typical paddy soil pH range. Recent works showed that Si release from phytoliths entrapped in aggregates decreased substantially (Li et al., 2022; Li et al., 2023). Thus far phytolith dissolution has been analyzed almost exclusively in laboratory environments while it is well established that mineral weathering rates measured in the laboratory and in the field can differ substantially (White and Brantley, 2003). Critically, phytolith dissolution is greatly influenced by environmental conditions such as pH, temperature, and water regime, which are rarely constant over time (Fraysse et al., 2009; Nguyen et al., 2019; Nguyen et al., 2021; Vander Linden et al., 2021).

Here, we present for the first time a field study on changes in phytolith solubility upon aging. We exposed phytoliths extracted from rice straw to ambient field conditions in paddy and non-paddy soils in the Philippines and Vietnam over a time period of up to 550 days. After recovery from soil, phytolith samples were analyzed for physical and chemical properties, as well as their dissolution kinetics. The main objectives of this study were to (i) explore phytolith dissolution rates under field conditions as a function of exposure time and differences between paddy and non-paddy soils, (ii) clarify the extent to which redox oscillations in paddy fields alter phytolith properties and promote development of inorganic/organic coatings, and (iii) test whether the observed changes in physical and chemical properties explain phytolith stabilization over time.
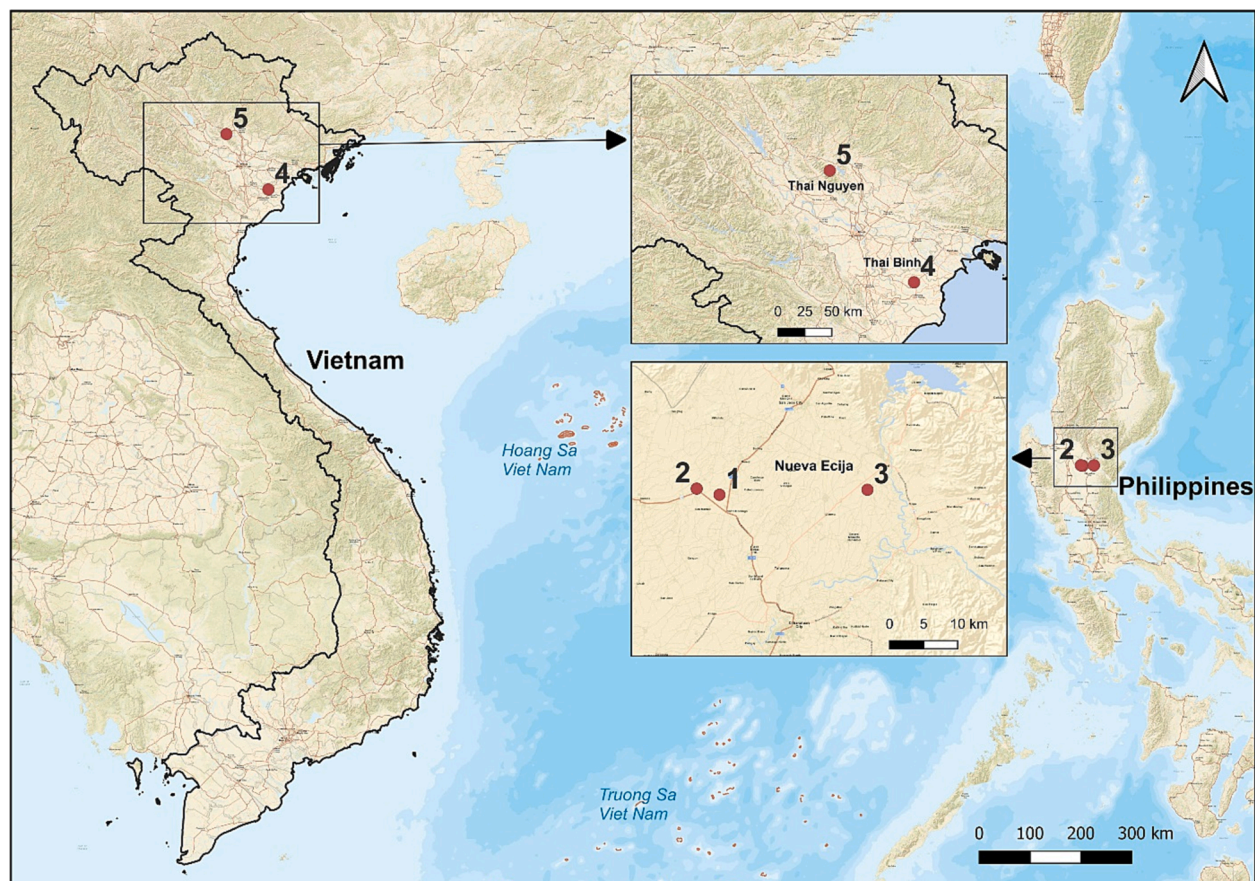
Fig. 1. Geographic location of the five study sites: 1 Maligaya, 2 Bunol, 3 Rizal, 4 Lien Giang, and 5 My Yen.

2. Materials and methods

2.1. Study sites

Field research was conducted at five study sites (Fig. 1), three in the Philippines ("Maligaya" at 15°39'59.1"N 120°52'32.6"E, "Bunol" at 15°40'29.2"N 120°50'40.4"E, and "Rizal" at 15°40'23.7"N 121°04'41.0"E), and two in Vietnam ("Lien Giang" at 20°35'17.9"N 106°20'31.8"E and "My Yen" at 21°34'36.3"N 105°35'38.9"E). Mean annual temperatures and precipitation of the study regions are shown in Fig. 2. The three sites in the Philippines are all located in the province of Nueva Ecija in the central plains of Luzon Island, between ca. 45 and 80 m above sea level. The climate of central Luzon is classified as monsoonal tropical (Am climate according to Köppen-Geiger classification, Peel et al., 2007). Dominant soil types are Gleyic Cambisols, Pellic Vertisols, and Dystric Nitisols (FAO, 1979; IUSS Working Group WRB, 2022). The two Vietnamese field sites are in two different regions in northern Vietnam. My Yen is situated in a hilly landscape next to the Tam Dao mountain range at ca. 110 m above sea level in the Thai Nguyen province. Dominant soil types are Orthic, Ferric, and Gleyic Acrisols (FAO, 1979; IUSS Working Group WRB, 2022). Lien Giang is located in the Red River Delta between the Red and the Thai Binh rivers at 0–5 m above sea level in Thai Binh province. The dominant soil types are Eutric Fluvisols and Eutric Gleysols (FAO, 1979; IUSS Working Group WRB, 2022). The climate of both Vietnamese regions is classified as humid subtropical (Cwa climate according to Köppen-Geiger classification, Peel et al., 2007). Lien Giang has a higher mean annual temperature, while My Yen has higher annual precipitation.

2.2. Preparation of phytolith material

Phytoliths were extracted from Philippine rice straw (*Oryza sativa* L. cv. NSIC Rc222) using a dry-ashing method (Parr et al., 2001). The straw was rinsed twice in a sonication bath using ultrapure water to remove soil residues. After drying at 50 °C, the straw was ground for 3 min using a ball mill. The material was then heated in a crucible at 500 °C for 5 h. After cooling, the ash was washed with 10 % HCl at 70 °C for 20 min. The material was placed on 0.45-µm polyethersulfone (PES) membranes (Pall Corporation, USA) and rinsed with ultrapure water to remove the acid. The obtained phytoliths were oven-dried at 40 °C for 24 h. After drying, 8 g of extracted phytoliths were placed in mineral bags that were made by fixing two sheets of nylon tissue with a mesh width of ca. 1 µm (PA-1/1, Franz-Eckert GmbH, Waldkirch, Germany) with the snap locking mechanism of round polypropylene jars with lids (500 ml, ø =112 mm, Semadeni AG, Königstein, Germany; see Figure A1).

2.3. Field experiment

At each study site, a pair of neighboring fields within maximal 100 m distance with contrasting management types were selected for phytolith incubation: A paddy rice field (hereafter denoted as "paddy") and a field with an alternative land use (denoted as "control"). While the precise land use of the control fields varied between study sites (see Appendix A: Supplementary Information, Table A1) and was not consistent over time due to individual farmers' decisions, they were all characterized by the absence of managed periodic flooding and drainage. In each of the plots, a section at the margin of the field was cordoned off for phytolith incubation. The sections were cultivated as usual, but no plowing or puddling was performed within the section containing phytoliths. Phytolith bags were buried in the topsoil at a depth of ca. 15 cm. The bags were placed along a transect at a distance of 1 m in between individual bags. At both ends of the transects, metal posts were placed to facilitate the recovery of the phytolith bags. In the Philippines field sites, a total of 12 bags were placed corresponding to triplicates of four time points for phytolith retrieval (T1–T4). These were defined as follows: T1 retrieved two weeks after rice transplantation (ca. two months after burial), T2 retrieved after one rice harvest, T3 retrieved after two rice harvests, and T4 after three rice harvests. The Vietnamese field sites followed the same design; but the total duration of the experiments was shorter. Here, a total of six bags corresponding to triplicates of two time points were buried. These were defined as follows: T2 retrieved after one rice harvest, T3 retrieved after two rice harvests. The actual dates of phytolith retrieval varied between study sites, reflecting the differences in rice development and farmers' decisions on harvesting times. Further details about field design, dates of phytolith burial, type of cultivation, and times of phytolith retrieval are summarized in Appendix A: Supplementary Information (Figures A1-A4, Table A1). Soil moisture regime during the experiment was recorded qualitatively during regular field visits and was converted to scores ranging from 1 to 6 based on the wording in the reports from these visits (see Figure A5 in Appendix A: Supplementary Information for details). Phytolith bags were recovered within intact soil monoliths such that the bags were not damaged during the process. Adhering soil materials were carefully removed and the bags were dried at 40 °C for 48 h and subsequently sealed in plastic bags for shipping to the laboratory.

2.4. Soil analyses

At each burial point of phytoliths, ca. 500 g of soil was collected and pooled as triplicates for analysis of basic soil properties. The soil was air-dried and sieved to < 2 mm. Soil pH was measured in 0.01 M CaCl$_2$ at 1:2.5 soil-to-solution ratio. Organic carbon was determined by dry combustion (Vario MAX Cube, Elementar Analysensysteme, Hanau,
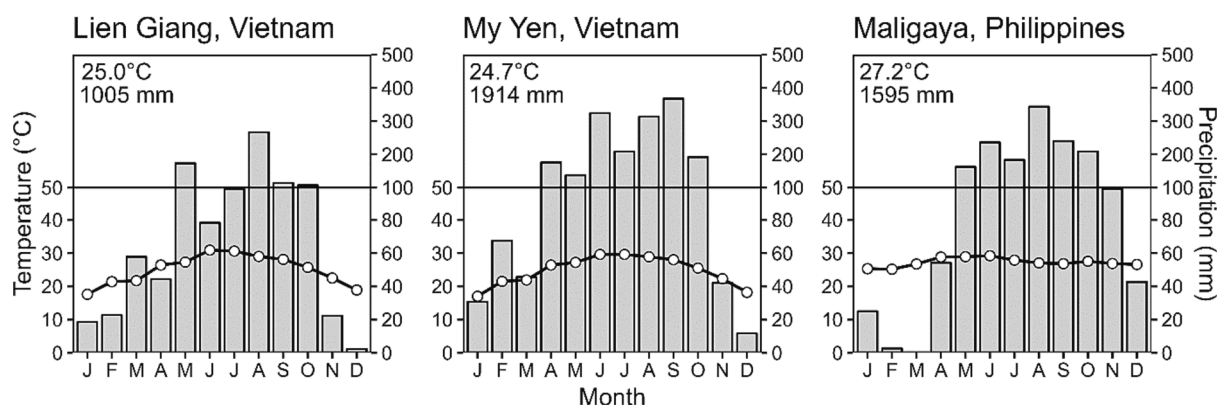
Fig. 2. Mean monthly temperatures (open circles) and precipitation (bars) in the study regions. Data for Maligaya are drawn from the central experiment station of the Philippine Rice Research Institute located in Maligaya for the year 2019, data for Lien Giang and My Yen are drawn from the Vietnam Meteorological and Hydrological Administration (VMHA) for the year 2019.

Germany). Prior analysis showed no evidence of inorganic carbon. Total pedogenic contents of Fe (Fe_d) and manganese (Mn_d) in pedogenic oxide phases were estimated by dithionite–citrate–bicarbonate extraction (Mehra and Jackson, 1958). Oxalate-extractable Fe (Fe_o) and Al (Al_o) were determined as measures of short-range ordered minerals and organically complexed forms (Schwertmann, 1964). The content of soluble and exchangeable Si (Si-Ac) was estimated by acetate extraction (Imaizumi and Yoshida, 1958), whereas immediately plant-available Si (Si-CaCl₂) was determined by $CaCl_2$ extraction (Haysom and Chapman, 1975). Concentrations of extracted Fe, Mn, Al, and Si were measured by inductively coupled plasma-optical emission spectroscopy (ICP-OES) (Ultima 2, Horiba Jobin-Yvon, Longjumeau, France). Soil texture was determined with the standard sieve-pipette method after removal of organic matter and Fe oxides (ISO, 2020).

2.5. Analyses of phytolith material

2.5.1. Phytolith recovery and mass loss

Field-exposed phytolith samples were recovered by gently opening the bags and removing the material from the bag's inside with a spatula. The recovered material was again oven-dried at 40 °C for 48 h and the remaining phytolith mass was determined gravimetrically. Particle size < 1 μm was negligible in the original phytolith sample, so we assumed that no phytolith material was lost by passage through the nylon mesh (see Appendix A: Supplementary information, Figure A6).

2.5.2. Microwave-assisted digestion and phytolith carbon content

Phytolith surface chemistry was assessed by microwave-assisted acid digestion. Aliquots of fresh and field-exposed phytolith material (0.15 g) were filled in Teflon tubes with 5 ml of 65 % HNO_3, 2 ml of 30 % hydrogen peroxide, and 3 ml of ultrapure water. The tubes were closed and placed into a microwave digestor (Mars 5, CEM Corporation, Charlotte, USA) with the microwave being heated to 180 °C using a 15-minute ramp. The final temperature was held constant for 10 min and the vessels were allowed to cool for 20 min. The digests were analyzed for Al, Fe, Ca, K, Mn, and Mg by ICP-OES. Phytolith carbon content was determined by dry combustion with the Vario MAX Cube for fresh phytoliths and phytoliths retrieved at the last time point.

2.5.3. X-ray photoelectron spectroscopy

Fresh phytoliths and phytoliths retrieved at the last time point were additionally studied by X-ray photoelectron spectroscopy (XPS) using an Axis Supra instrument (Kratos Analytical, Manchester, UK). Aliquots of phytoliths were gently pressed into indium foil and three individual spots were analyzed for each sample, using a monochromatic Al-Kα source (photon energy 1486.6 eV). For each spot (300 × 700 μm), we obtained survey scans at 14 mA emission current and a pass energy of 160 eV using of 4 sweeps of 150 s sweep time and a step size of 0.5 eV. Survey spectra were processed using Casa XPS software (CasaXPS Version 2.323PR1.0, Casa Software Ltd, Cheshire, UK). All spectra were charge corrected using the C 1s peak at 284.8 eV as reference. Five spectral regions were defined for quantification, representing the transitions Fe 2p (704.5–727.0 eV), O 1s (526.2–540.4 eV), C 1s (277.4–292.8 eV), Si 2p (97.8–111.4 eV), and Al 2p (69.8–82.5 eV). After subtraction of a Shirley-type background, element intensities were computed from resulting peak areas weighted by the respective relative sensitivity factor. Uncertainties of the resulting peak areas were estimated by computing the standard deviation (σ) of the peak areas using a Monte Carlo approach in Casa XPS. Averaged 2σ was used as the approximated detection limit. In contrast to element contents obtained by microwave digestion, XPS reveals the chemical composition only within a depth of max. 10 nm, thus is best suited to detect the formation of surface coatings on phytolith surfaces.

2.5.4. Specific surface area and surface charge

The specific surface area (SSA) of fresh and field-exposed phytoliths

was derived from N_2 adsorption isotherms obtained at 77 K using an Autosorb IQ MP instrument (Quantachrome Instruments, Boynton Beach, USA). The SSA was calculated with the BET equation (Brunauer et al., 1938) using 11 adsorption points at relative pressures p/p0 between 0.05 and 0.35. The zeta (ζ) potential of phytoliths was obtained by measuring the electrophoretic mobility of suspended phytoliths by dynamic light scattering (Zetasizer Nano ZS, Malvern Panalytical, Malvern, UK). Phytoliths (~2 mg) were suspended in 25 ml of 0.01 M NaCl adjusted to pH 7, and 1 ml of the settled suspension was pipetted into a measuring cuvette. Three ζ measurements per sample were made within five minutes. The ζ potential was derived from the electrophoretic mobility using the Smoluchowski equation (Sze et al., 2003).

2.5.5. Particle size

Fresh phytoliths as well those retrieved at the last time point were analyzed with a laser diffraction analyzer equipped with a wet dispersion unit (Helos/KR + Quixel, Sympatec GmbH, Clausthal-Zellerfeld, Germany) to measure their particle size distribution (ISO, 2009). Each sample was pretreated with 0.05 M sodium pyrophosphate ($Na_4P_2O_7$ •10 H_2O) to support dispersion. Before laser diffraction analyses of 3 g with a helium–neon light source (wavelength: 632.8 nm), samples were dispersed by sonication (60 s at 60 W). The diffraction of light by a single particle is described mathematically by the Fraunhofer theory. In total, 48 size classes between 0.5 and 3500 μm were obtained in order to derive the median particle size (PSD_{50}).

2.5.6. Phytolith solubility

A standardized batch dissolution experiment was performed in order to measure Si release from fresh and field-exposed phytoliths. In total, six batches of triplicate phytoliths (each 20 mg) were suspended in 10 ml 0.01 M $CaCl_2$ solution adjusted to pH 6.5. Suspensions were kept in plastic vials and placed in the dark on a laboratory shaker at 25 °C set to 200 rpm. After 1, 3, 7, 14, 28, and 56 days, suspensions were filtered to < 0.45 μm for ICP-OES measurement of Si. The Si release was described by Equation (1), where k is the rate constant, C the Si concentration, C_{eq} the Si concentration at equilibrium, and t is time.

$$C = C_{eq}\left(1 - e^{-kt}\right) \tag{1}$$

The maximum dissolution rate (R_{max}) was determined at t = 0 where $R_{max} = kC_{eq}$. Dissolution rates and Si equilibrium concentrations were computed by fitting Equation (1) to measured Si concentrations using the non-linear least squares solver "curve_fit" from the SciPy Python library.

2.6. Statistical analyses

Statistical analyses were conducted with RStudio (Version 4.1.2, R Core Team, 2021) unless stated otherwise. All experimental data were tested for normal distribution (Shapiro-Wilk test) and homogeneity of variance (Levene's test) followed by analysis of variance (one-way ANOVA) and Tukey's HSD (honestly significant differences) for multiple pairwise comparisons. XPS-derived Al concentrations were log transformed to fulfill the normality requirement. For non-normal and heteroskedastic data, a Kruskal-Wallis test was used, followed by pairwise Wilcoxon test. For soil chemical data, Student's t-test was used to compare means between paddy and control soils, as well as between Vietnam and the Philippines. Correlations between different variables were tested with Pearson's correlation coefficient for normally distributed data and Spearman's rank correlation coefficient for non-normal data. Assumed steady mass loss rates in the field were estimated with multiple linear regression with the variables time and management (2 levels), and their interaction term using the lm function in R. Plots were generated using SigmaPlot (Version 11.0, Systat Software Inc., USA) and R.

3. Results and discussion

3.1. Soil characteristics

Basic soil properties of the topsoils (0–15 cm) for each study site are shown in Table 1. With the exception of Rizal, the neighboring pairs of paddy and control fields at each location had similar basic properties. Soil textures of paddy soils classified according to Blum et al. (2018) comprised sandy loam (My Yen), loam (Bunol), clay loam (Maligaya and Rizal), and silty loam (Lien Giang). Corresponding control soils had the same texture in My Yen, Lien Giang, and Bunol. In Maligaya the control soil the texture was classified as a loam and in Rizal as a sandy loam. Soil pH ranged from acidic (pH 4.3) to neutral (pH 6.8), with the majority of fields being between pH 4–6. There were no significant differences between paddy and control soils. Total organic C in the investigated soil samples ranged from 6.6 to 17.3 g kg^{-1} with no significant differences between paddy and control soils. Oxalate-extractable Fe and Al ranged from 1.3 to 6.3 g kg^{-1} and 0.4 to 1.2 g kg^{-1}, respectively. Paddy soils had significantly higher Fe$_o$ contents than the corresponding control soils (t-test, p < 0.05), while Al$_o$ was not significantly different between management types. Both fields in My Yen and the control field in Rizal had very low contents of both, Fe$_o$ and Al$_o$, in line with their coarse textures. Dithionite-extractable Fe ranged from 3.8 to 19.2 g kg^{-1} with the smallest values detected in My Yen and the control field in Rizal. Soils in Bunol had also relatively low Fe$_d$ contents, while the remaining soils had similar Fe$_d$ contents. There were no significant differences between paddy and control soils. Dithionite-extractable Mn ranged from 0.1 to 0.8 g kg^{-1}. Soils in My Yen had significantly lower Mn$_d$ contents compared to other fields, whereas the paddy fields in Maligaya and Bunol had the highest Mn$_d$ contents. While there was no statistically significant difference between paddy and control soils overall, pairwise comparisons (Tukey HSD) showed that Mn$_d$ was higher in control fields in most locations. Additionally, Philippine soils had significantly more Mn$_d$ than Vietnamese soils (t-test, p < 0.05). Acetate- and CaCl$_2$-extractable Si ranged from 17.2 to 136.0 mg g^{-1} and 8.1 to 101.0 mg g^{-1}, respectively. Results from both extractions were strongly positively correlated (r = 0.85, p < 0.001), with Si-Ac being between 1.3 and 7.5 times higher than Si-CaCl$_2$. This is consistent with previous work stating that CaCl$_2$ extracts the immediately plant- available Si, while acetate extracts soluble and some exchangeable Si (Sauer et al., 2006). Philippine soils showed a significantly higher Si contents than Vietnamese soils for both Si-Ac and Si-CaCl$_2$ (t-test, p < 0.05). Overall, there was no statistically significant difference between paddy and control soils, however pairwise comparisons showed that Si-CaCl$_2$ was consistently lower in paddy soils compared to their corresponding controls (although not statistically significant in Bunol and My Yen).

3.2. Phytolith mass balance and field-based dissolution rates

During field-exposure, up to 29 % of the initial phytolith mass was lost, with phytoliths exposed in paddy soils being dissolved much faster than those from the control soils (Fig. 3). Data for the first retrieval (T1, Philippine soils) show that dissolution was initially very fast and slowed then rapidly. Comparison with later time points suggests that the dissolution rate did not decrease substantially throughout the remaining time in paddy soil. The slower dissolution of phytoliths exposed in control soils showed pronounced differences between individual sites. For example, phytoliths buried in the Maligaya soil lost only 2.8 ± 0.3 % of their initial mass after 519 days, while in Bunol 15.7 ± 0.1 % were lost after 549 days. It should be noted that there was an irrigation leakage at Bunol around 102 days after burial, causing standing water in the control field. That might explain the greater dissolution at this location. As in the paddy fields, data for the first retrieval suggests an initially faster dissolution, later converging to a steady rate.

The assumed steady rates for phytoliths exposed in paddy and control soils were estimated by multiple linear regression using time (x) and management as independent variables and allowing for interactions. Data was only fitted between the first and last retrieval time (i.e. the origin was omitted), therefore the initial phase of rapid dissolution was disregarded. The resulting linear regression was y = 0.035 + 0.0001x + 0.028 M + (0.0002Mx) (adjusted r^2 = 0.67, p < 0.001), where M is a dummy-coded variable for the management type with the value 0 for control and 1 for paddy, respectively. The resulting rates were 0.34 ± 0.04 mg g^{-1} d^{-1} for paddy soils and 0.11 ± 0.04 mg g^{-1} d^{-1} for the control soils, indicating that phytoliths dissolved more than three times faster in paddy soils. This is likely caused by the different water regimes

Table 1
Selected properties of topsoils (0–15 cm) at the different field sites. Values are given as mean and standard deviation (in parentheses). Means not sharing any letters are significantly different by ANOVA. Abbreviations: C$_{org}$ is total organic C, Al$_o$ and Fe$_o$ are oxalate-extractable Al and Fe, respectively; Fe$_d$ and Mn$_d$ are dithionite-extractable Fe and Mn, respectively; Si-Ac and Si-CaCl$_2$ are acetate and CaCl$_2$-extractable Si, respectively.

Location	Philippines						Vietnam			
	Maligaya		Bunol		Rizal		Lien Giang		My Yen	
Management	Paddy	Control	Paddy	Control	Paddy	Control	Paddy	Control	Paddy	Control
Sand (%)	20.5	37.3	39.9	35.1	23.6	54.7	2.3	4.1	54.1	54.9
N = 2	(1.3)	(0.4)	(2.5)	(3.5)	(4.8)	(0.1)	(0.4)	(0.2)	(0.9)	(1.4)
Silt (%)	50.4	40.8	43.8	41.5	42.8	32.5	69.3	71.8	32.6	31.9
N = 2	(0.5)	(1.7)	(1.5)	(1.7)	(2.8)	(0.1)	(0.7)	(1.4)	(0.2)	(1.4)
Clay (%)	29.1	21.9	16.3	23.4	33.6	12.8	28.4	24.1	13.3	13.3
N = 2	(0.8)	(1.2)	(1.0)	(0.2)	(2.0)	(0.1)	(1.1)	(1.5)	(1.1)	(0.0)
pH (CaCl$_2$)	5.6 ^{cd}	5.4 ^{cd}	4.5 ^{ab}	5.0 ^{abc}	4.3 ^{a}	6.8 ^{d}	6.1 ^{d}	5.3 ^{cd}	4.4 ^{a}	5.2 ^{bc}
N = 3	(0.2)	(0.1)	(0.3)	(0.0)	(0.3)	(0.1)	(0.2)	(0.3)	(0.0)	(0.1)
C$_{org}$ (g kg^{-1})	12.8 ^{abc}	16.0 ^{c}	9.0 ^{ab}	6.6 ^{a}	13.7 ^{bc}	17.3 ^{c}	13.9 ^{bc}	13.8 ^{bc}	13.7 ^{bc}	11.8 ^{abc}
N = 3	(0.6)	(0.0)	(0.5)	(0.2)	(3.8)	(0.5)	(2.0)	(1.5)	(0.7)	(0.8)
Al$_o$ (g kg^{-1})	0.6 ^{b}	0.6 ^{b}	1.0 ^{d}	1.2 ^{e}	0.6 ^{b}	0.5 ^{a}	0.6 ^{b}	0.8 ^{c}	0.4 ^{a}	0.6 ^{b}
N = 3	(0.0)	(0.0)	(0.0)	(0.1)	(0.0)	(0.0)	(0.0)	(0.1)	(0.0)	(0.0)
Fe$_o$ (g kg^{-1})	7.2 ^{d}	4.9 ^{bcd}	5.7 ^{bcd}	3.6 ^{ab}	6.3 ^{cd}	1.3 ^{a}	6.1 ^{cd}	4.5 ^{bc}	1.9 ^{a}	1.5 ^{a}
N = 3	(0.0)	(0.1)	(0.1)	(0.2)	(1.9)	(0.0)	(0.5)	(0.2)	(0.5)	(0.1)
Fe$_d$ (g kg^{-1})	18.0 ^{cd}	17.3 ^{bcd}	9.9 ^{abc}	9.9 ^{abc}	18.7 ^{d}	8.6 ^{ab}	19.2 ^{d}	19.5 ^{d}	3.8 ^{a}	9.0 ^{ab}
N = 3	(0.1)	(0.9)	(0.2)	(0.3)	(2.9)	(0.2)	(0.3)	(1.5)	(0.2)	(3.0)
Mn$_d$ (g kg^{-1})	0.3 ^{bc}	0.7 ^{ef}	0.6 ^{de}	0.8 ^{f}	0.4 ^{cd}	0.5 ^{d}	0.2 ^{b}	0.6 ^{de}	0.1 ^{a}	0.1 ^{a}
N = 3	(0.0)	(0.0)	(0.1)	(0.0)	(0.1)	(0.1)	(0.0)	(0.0)	(0.0)	(0.0)
Si-Ac (mg kg^{-1})	108.7 ^{d}	112.0 ^{de}	71.3 ^{bc}	90.0 ^{cd}	115.3 ^{ef}	136.0 ^{f}	75.7 ^{bc}	61.4 ^{b}	17.2 ^{a}	27.3 ^{a}
N = 3	(1.5)	(5.0)	(8.5)	(1.0)	(8.0)	(0.0)	(6.2)	(12.4)	(1.6)	(4.5)
Si-CaCl$_2$ (mg kg^{-1})	48.3 ^{bc}	76.0 ^{d}	47.7 ^{bc}	61.6 ^{cd}	61.7 ^{cd}	101.0 ^{e}	10.4 ^{a}	38.2 ^{b}	8.1 ^{a}	12.5 ^{a}
N = 3	(2.5)	(4.0)	(4.6)	(0.7)	(9.7)	(9.0)	(4.7)	(5.6)	(0.7)	(0.5)
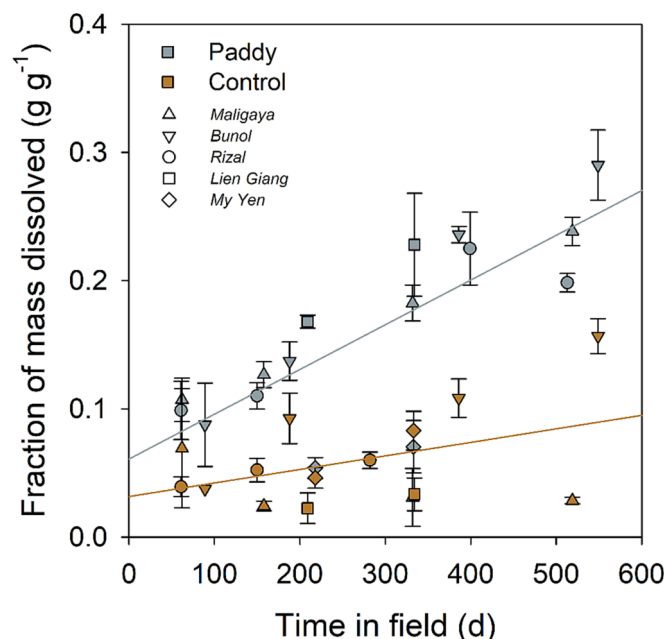
Fig. 3. Phytolith mass balance over time in paddy and non-paddy control soils. Data are mean values ± standard deviation. Solid lines represent the multiple linear regression y = 0.04 + 0.0001x + 0.03 M + (0.0002Mx), with M = 0 for control soils and M = 1 for paddy soils (adjusted r^2 = 0.67, p < 0.001).

of paddy and control fields. As water replaces air from soil pores during waterlogging, phytolith surfaces are permanently wetted and exposed to weathering. The increased hydraulic conductivity in the saturated pore space additionally facilitates the removal of released Si, thereby increasing the concentration gradient between phytolith surface and pore water. Dissolved Si can be lost due to leaching (Nguyen et al., 2016) or plant uptake. This is corroborated by consistently lower Si-CaCl$_2$ contents in the paddy soils. Another potential mechanism explaining higher phytolith dissolution in paddy soils is given by the common observation that in acidic soils, waterlogging is often accompanied with increasing pH (Kögel-Knabner et al., 2010; Sahrawat, 2005). While monitoring of redox potential and pH during field experiments was beyond the scope of this study, this possibility should not be neglected, given the strong pH dependence of phytolith dissolution (Fraysse et al., 2006).

The variation of dissolution rates among the paddy fields was lower than among control fields with the exception of the paddy field in My Yen, where the dissolution resembled that of the control fields. We suppose that this was due to the coarse texture of that paddy field. Under waterlogged conditions, water movement through the bags filled with silt-sized phytoliths with lower saturated hydraulic conductivity was probably restricted. However, overall, our data consistently suggest a much faster dissolution of phytoliths in soils subjected to flooding than in soils without water submergence. Comparison of mass balance data with measured soil parameters revealed no meaningful relationships that might explain site-dependent variations in solubility (data not shown).
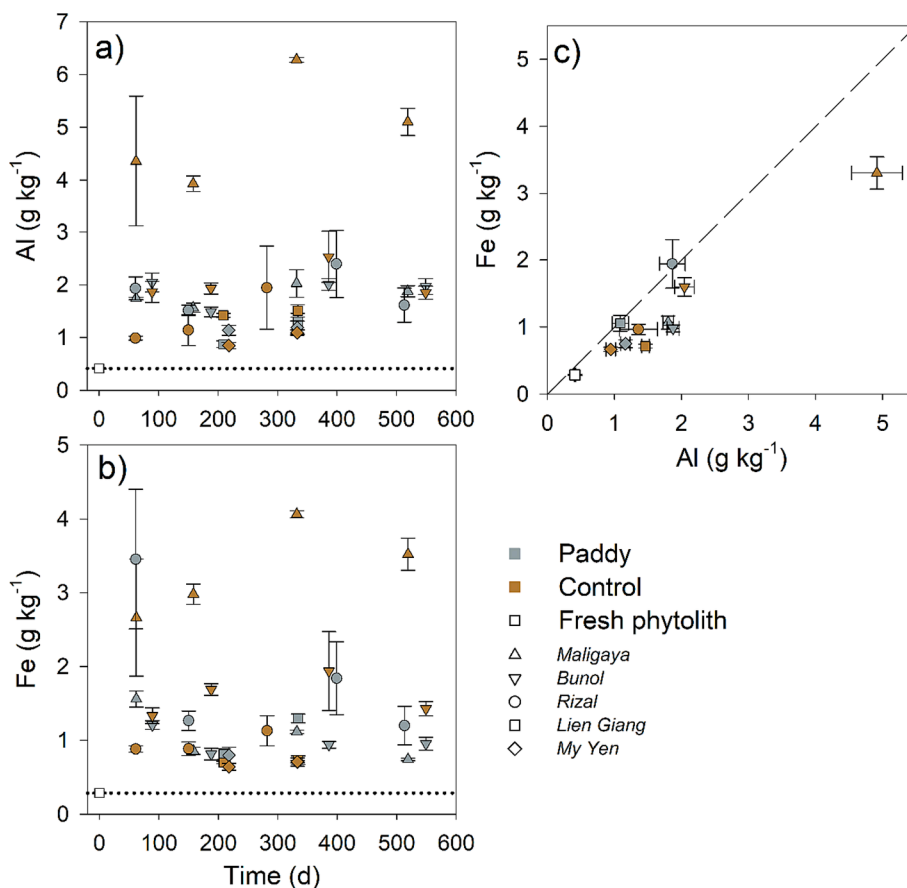
Fig. 4. Nitric acid–hydrogen peroxide-extractable Fe and Al from rice phytoliths exposed to ambient topsoil conditions for up to 1.5 years. (a) Al, (b) Fe, (c) average Fe vs. Al across all time points for each location. The dashed line in (c) represents the 1:1 relationship. Dotted line in (a) and (b) represents the average concentration for fresh phytoliths. Data are presented as mean values ± standard deviations.

3.3. Phytolith surface chemistry

Fig. 4 shows the amounts of Fe and Al extracted by the microwave-assisted acid digestion from phytoliths. Fresh phytolith Fe and Al content was 0.3 ± 0.0 g kg^{-1} and 0.4 ± 0.0 g kg^{-1}, respectively. Both, Fe and Al contents increased immediately upon field exposure with little variation over the course of the exposure period. Accumulation of Fe and Al on phytolith surfaces were within a narrow range (ca. 1–2 g kg^{-1}), with the notable exception of the control site in Maligaya, showing contents about twice of the other sites, and the paddy field in Rizal with elevated Fe contents after the first retrieval. Increases in Fe and Al were statistically significant for phytolith endmembers (fresh phytoliths and phytoliths retrieved at the last time point; Kruskal-Wallis test, p < 0.05) but there was no significant difference between paddy and control fields in either Fe or Al content (pairwise Wilcoxon test; Fe: p = 0.25, Al: p = 0.53). This is surprising since oxalate-extractable Fe contents in topsoils of paddy soils were higher than in the control soils across all locations (Table 1), suggesting more active Fe capable to interact with phytolith surfaces. We have shown in laboratory experiments, that phytoliths accumulated Fe from soil solutions obtained under oscillating redox conditions but not from solutions obtained under constant oxic conditions (Koebernick et al., 2022). However, the time scale of these experiments differed vastly as the maximum exposure time was 12 h, compared to the minimum exposure of 61 days in the field. Additionally, our laboratory experiments used soil solutions without other mineral phases apart from phytoliths being present.

For the field-exposed phytoliths, acid-extractable Fe and Al contents were strongly positively correlated (Fig. 4c, $\rho = 0.76$, p < 0.001), which suggests a similar accumulation mechanism. This is hardly compatible with the hypothesis of sorption of Fe or Al from soil solution since both elements are expected to be available under different soil conditions. A possible explanation is the retention of organo-metallic complexes or organic-rich Fe and Al bearing mineral colloids by phytolith surfaces, as both, acid-extractable Fe and Al were positively correlated with total phytolith C ($\rho = 0.52$, p < 0.01 for Fe, $\rho = 0.48$, p < 0.01 for Al). In contrast to Fe and Al, the amount of extractable Mn was very low (data not shown). Extractable Mn of fresh phytoliths was 0.1 ± 0.0 g kg^{-1}, and there was no detectable accumulation of Mn after exposure to soil.

Field exposure led to an increase in total phytolith C content from 1.5 ± 0.3 g kg^{-1} for fresh phytoliths to 2.3 ± 0.6 g kg^{-1} in paddy soils and 2.3 ± 0.3 g kg^{-1} in control soils (Kruskal-Wallis test, p < 0.05). The difference between paddy and control soils was not significant (pairwise Wilcoxon test, p = 0.90).

Analyses of phytolith endmembers (fresh phytoliths and phytoliths retrieved at the last time points) with XPS showed that all phytoliths were little coated with solution-derived compounds, even after exposure to ambient field conditions for up to 1.5 years (Fig. 5a). Fresh phytoliths had a surface elemental composition of 68.2 ± 0.4 at% O, 30.6 ± 0.1 at% Si, 0.9 ± 0.3 at% C, and 0.2 ± 0.1 at% Al (barely above the estimated detection limit of $2\sigma = 0.2$ at%). Surface Fe concentration was below the estimated detection limit of $2\sigma = 0.1$ at%. Fresh phytoliths also showed a small K signal, which was omitted in the quantification. For all field-exposed phytoliths, C increased to concentrations ranging between 3.5 ± 0.5 at% (Maligaya, paddy) and 9.3 ± 4.8 at% (Maligaya, control). Surface C concentration significantly increased in the order fresh < paddy < control phytoliths (Kruskal Wallis test p < 0.05, followed by pairwise Wilcoxon test p < 0.05 for any pairwise comparison). Surface Al concentrations of field-exposed phytoliths ranged between 0.2 ± 0.1 at% (My Yen, paddy) and 1.0 ± 0.0 at% (Maligaya, control). Mean surface Al concentration was highest for phytoliths from control fields, but there was no significant difference between phytoliths from paddy fields and fresh phytoliths (ANOVA, p < 0.05, followed by Tukey HSD). There was a significant positive correlation between Al and C ($\rho = 0.55$, p < 0.01, Fig. 5b). Surface Fe concentrations remained below the detection limit for all samples, except for the control fields in Maligaya (0.2 ± 0.0 at%) and Bunol (0.1 ± 0.0 at%).

In summary and in contrast to the acid digestion results, XPS analyses suggest that phytolith surfaces exposed in paddy fields had less accumulation of Fe, Al, and C than phytoliths exposed in control soils. The discrepancy between XPS and acid digestion results might be explained by the different surface sensitivity of both techniques. Acid digestion might release Fe and Al from pores within phytoliths and between aggregated phytoliths, whereas XPS measures only the external ~ 10 nm of the phytolith surfaces. Overall, both methods yield compatible results showing that although phytoliths were exposed to ambient soil conditions, including redox oscillations, the extent of surface coatings was rather limited. Strikingly, the only samples with significant Fe concentrations were those exposed in control fields, clearly demonstrating that redox oscillations do not necessarily induce Fe accumulation on phytolith surfaces in paddy fields. Consequently, phytolith surface chemistry was not related to mass loss in the field.

3.4. Phytolith surface area, particle size, and ζ potential

Phytolith endmember's (fresh phytoliths and phytoliths retrieved at the last time points) SSA, PSD$_{50}$, and ζ-potential at pH 7 are summarized in Table 2. Despite the significant dissolution of up to almost 30 % of phytoliths the changes in phytolith morphology were little. Both SSA
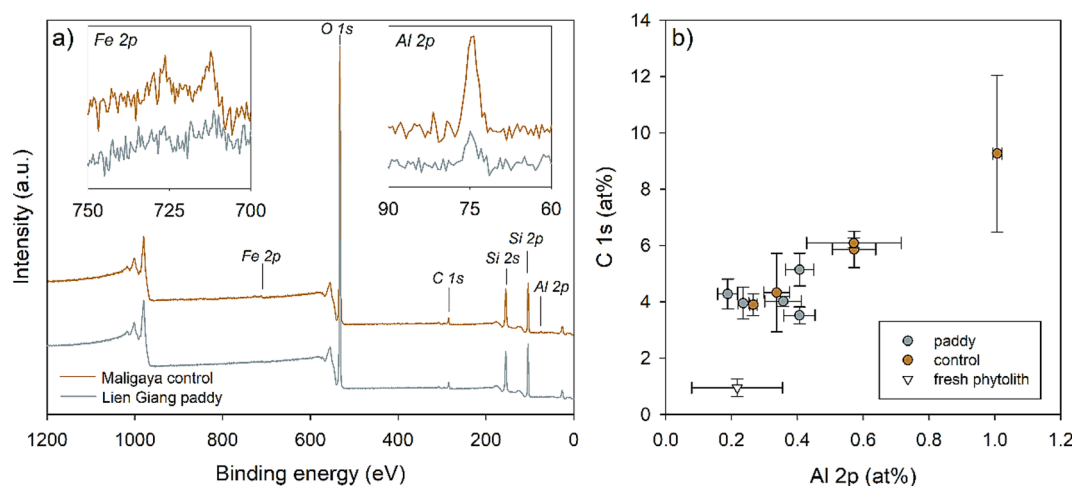
Fig. 5. X-ray photoelectron spectroscopy of phytolith endmembers (fresh phytoliths and phytoliths retrieved at the last time points). (a) XPS survey spectra from two selected rice phytolith samples. (b) phytolith surface C and Al concentrations plotted over Al. Inlets in (a) show enlarged sections of the survey spectra at the Fe 2p and the Al 2p lines, respectively. Error bars in (b) depict standard errors of n = 3 measurements.

Table 2

Morphological and surface charge characteristics of rice phytolith endmembers (fresh phytoliths and phytoliths retrieved at the last time points). SSA is the specific surface area, PSD_{50} is the median particle size, ζ pH 7 is the ζ-potential measured at pH 7. Data are given as mean $\pm$ standard deviation. Different letters indicate a significant difference by ANOVA / Kruskal-Wallis test at the 5 % level of significance.

	SSA ($m^2 g^{-1}$)	PSD_{50} (μm)	ζ pH 7 (mV)
Fresh phytolith	76.93 ± 2.23^a	40.67 ± 0.61^a	-32.51 ± 1.07^a
Paddy	70.99 ± 6.56^a	37.53 ± 1.99^a	-36.00 ± 3.85^a
Control	76.11 ± 6.44^a	38.10 ± 3.71^a	-36.07 ± 3.86^a

and PSD_{50} showed no significant changes according to ANOVA over the incubation period (SSA p = 0.07; PSD_{50} p = 0.37). The full particle size distributions indicated an overall decrease in particle size, which was (in most of the samples) accompanied by an enrichment of the largest particles of $\varnothing > 100 \ \mu m$ (Fig. 6). While the effect was little, it is consistent with the notion that particles with a smaller surface to bulk ratio are more stable against dissolution as suggested by Cabanes and Shahack-Gross (2015). The ζ potential at pH 7 showed no significant differences between fresh and exposed phytoliths (Kruskal-Wallis test, p = 0.18).

3.5. Phytolith solubility experiments

During controlled batch dissolution experiments, the pH of the $CaCl_2$ solution decreased from pH 7 to pH 6.5 ± 0.2 after one day and then stabilized (pH after 56 days was 6.4 ± 0.2). While most samples were within a narrow pH range there were two exceptions. For fresh phytoliths, pH decreased to 5.9 ± 0.1, probably caused by residual acidity from the acid extraction, and in phytoliths from the Lien Giang paddy field at retrieval time T2, the pH was 6.9 ± 0.2. The development of Si concentrations during the dissolution experiment is shown in Fig. 6 for fresh phytoliths and the samples from Maligaya paddy (Fig. 7a) and control (Fig. 7b) fields, respectively. Fresh phytoliths were close to equilibrium concentration after 28 days, while field-exposed phytoliths dissolved slower, approaching near-equilibrium after 56 days. The fitted equilibrium concentration, C_{eq}, and the fitted maximum Si release rate, R_{max}, are plotted over time of exposure in the field in Fig. 7c and Fig. 7d, respectively. The results show that both C_{eq} and R_{max} decreased with
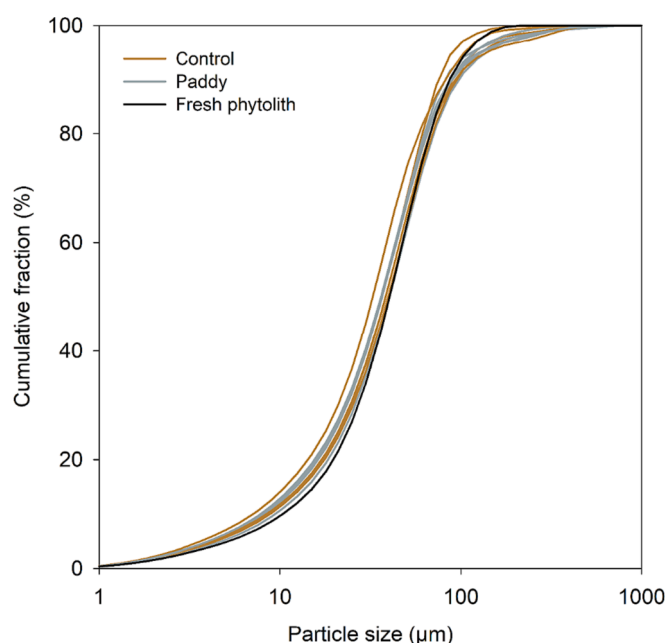
Fig. 6. Cumulative particle size distributions of phytolith endmembers.

exposure time in the field (note, the two variables are not independent, as $R_{max} = kC_{eq}$) for both paddy and control soils. The RMSE of individual fits was between 0.059 and 0.176 mM (average RMSE = 0.11 mM), indicating that the fits were reasonable and that the decrease of C_{eq} and R_{max} with exposure time is not an artefact of the fitting procedure. Interestingly, there was no systematic difference between soil management types, although the samples from the paddy fields had lost significantly more mass. The lack of significant changes in PSD_{50} and SSA of exposed phytoliths seems to suggest that changes in morphology were not the major cause of decreased solubility. In fact, particle size distributions showed an overall decrease in particle size, contrary to previous findings that showed a loss in small particles after dissolution treatments (Liu et al., 2023). An potential explanation could be the dissolution of fine surface features that would not lead to changes in particle size distributions or SSA, as was suggested by Fraysse et al. (2009).

An alternative mechanism that might explain the decrease in dissolution kinetics with time is the development of mineral and/or organic coatings on the phytolith surfaces, which may result in partial surface passivation through the blocking of reactive silanol sites, surface precipitation of oxides, and by promoting the aggregation of phytoliths due to opposing charge of Fe/Al oxides and phytoliths. This has often been suggested (e.g. Bartoli, 1985; Bartoli and Wilding, 1980; Wickramasinghe and Rowell, 2006) and we have recently shown that Fe oxide coatings may develop rapidly under oscillating redox conditions and are accompanied by decreasing rates of Si release from phytolith (Koebernick et al., 2022). The present field data show that phytoliths initially rapidly accumulated Al and Fe regardless of redox conditions with little changes during field exposure. Fitted R_{max} values were significantly negatively correlated with acid-extractable Al content ($\rho = -0.36$, p < 0.05) but not with Fe content ($\rho = -0.14$, p = 0.44). Comparison of R_{max} derived from laboratory measurements (2.7 to 12.3 mg g^{-1} d^{-1}, Fig. 6d) with the dissolution rates derived from mass loss in the field (0.34 ± 0.04 mg g^{-1} d^{-1} for paddy soils and 0.11 ± 0.04 mg g^{-1} d^{-1} for control soils, Fig. 3) shows that these rates differ by an order of magnitude.

This is not altogether surprising, as R_{max} was assessed under optimal and controlled conditions (e.g., complete wetting, low solid-to-solution ratio, constant agitation, maximum degree of undersaturation), therefore R_{max} can be interpreted as a potential dissolution rate. The differences in methodological approaches should be reflected when comparing phytolith dissolution rates with values from the literature. Many authors have provided phytolith half-life times, which can be calculated from the mass balance by $t_{1/2} = \frac{m_0}{2R}$, where the initial mass m_0 is 1 and R is the rate of mass loss (d^{-1}). The so-calculated half-life times using our field data are 4 years in paddy soils and 12.5 years in control soils. For comparison, Alexandre et al. (1994) estimated $t_{1/2}$ between 0.5 months and 9 months in the litter layer of a tropical rainforest. In temperate forests, Bartoli and Souchier (1978) found half-lives between 1 and 5 years in the litter layer and 0.5 – 150 years in the topsoils. In temperate North American grasslands, Blecker et al. (2006) found $t_{1/2}$ between 125 and 650 years, showing that phytolith dissolution increased with mean annual precipitation. Using a laboratory approach, Fraysse et al. (2009) found $t_{1/2}$ between 0.5 and 3 years for horsetail and larch phytoliths at pH 4 – 5, and $t_{1/2} < 100$ days at pH 6. These latter, much shorter half-life times are comparable to the values derived from laboratory dissolution rates in this work (between 41 and 188 days at pH 6.5), and in a previous laboratory study (between 33 and 103 days at pH $\sim$ 7, Koebernick et al., 2022). This illustrates that laboratory derived phytolith dissolution rates have only limited meaning in assessing the Si cycle in paddy fields (and beyond), underlining the need for more field studies.

3.6. Implications and conclusions

The most surprising result of this study is that the redox oscillations
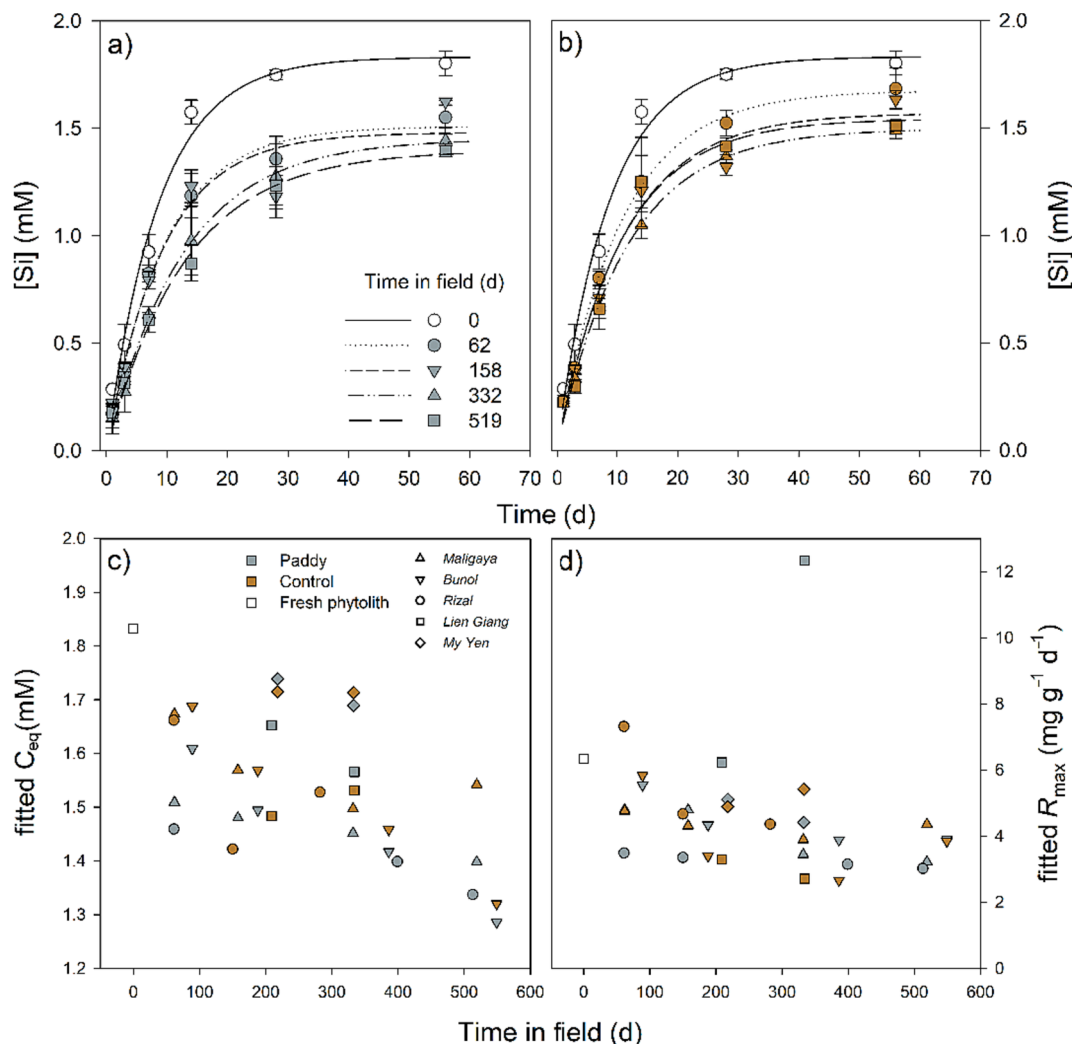
Fig. 7. Results from phytolith batch dissolution experiment. (a) Maligaya paddy soil, (b) Maligaya control soil, (c) fitted Si equilibrium concentration C_{eq}, and (d) fitted maximum Si release rate R_{max}.

induced by paddy cultivation had no significant effect on phytolith morphology, surface chemistry, and dissolution kinetics in the laboratory. In particular, there was no significant increase in Fe content with time under paddy cultivation. The total amount of Fe extracted from phytoliths incubated in paddy fields after up to 550 days in this study was smaller than the amount we extracted from phytoliths incubated in interchanging oxic–anoxic soil solutions in the laboratory for 12 h (Koebernick et al., 2022). We therefore conclude that Fe coatings on phytolith surfaces are not stable under submerged conditions. Additionally, we found no evidence that Fe accumulation decreases Si release rates. While Al content was found to be negatively correlated with Si release rate, this was only found to be true for laboratory derived potential Si release rates. Overall, our field exposure study suggests that formation of surface coatings is likely only a minor factor explaining the stability of soil phytoliths. Rather, phytolith stability is overwhelmingly governed by the water regime, which is in agreement with previous findings (Blecker et al., 2006). This is evidenced by much faster dissolution of phytoliths in paddy fields compared to fields without recurring periods of waterlogging. Phytolith dissolution in paddy fields during fallow periods should resemble those of the control fields. Therefore, standard paddy management seems well suited to support Si supply for rice cultivation, largely preserving phytoliths for the following growth period. We infer that, while laboratory experiments can be great tools for elucidating specific mechanisms, dissolution rates derived in the laboratory may severely overestimate phytolith dissolution. This underlines the importance of field studies for deriving realistic dissolution of phytoliths.

CRediT authorship contribution statement

Nicolai Koebernick: Conceptualization, Data curation, Formal analysis, Investigation, Methodology, Project administration, Resources, Validation, Visualization, Writing – original draft, Writing – review & editing. **Robert Mikutta:** Conceptualization, Funding acquisition, Methodology, Project administration, Writing – review & editing. **Klaus Kaiser:** Conceptualization, Funding acquisition, Investigation, Methodology, Project administration, Writing – review & editing. **Anika Klotzbücher:** Conceptualization, Investigation, Methodology, Project administration, Writing – review & editing. **Anh T.Q. Nguyen:** Investigation, Methodology, Resources, Validation, Visualization, Writing – review & editing. **Minh N. Nguyen:** Conceptualization, Investigation, Methodology, Resources, Writing – review & editing. **Thimo Klotzbücher:** Conceptualization, Formal analysis, Funding acquisition, Investigation, Methodology, Project administration, Visualization, Writing – review & editing.

Declaration of competing interest

The authors declare the following financial interests/personal relationships which may be considered as potential competing interests: Nicolai Koebernick reports financial support was provided by German Research Foundation. If there are other authors, they declare that they have no known competing financial interests or personal relationships that could have appeared to influence the work reported in this paper.

Data availability

Data will be made available on request.

Acknowledgements

Appendix A. Supplementary data

Supplementary data to this article can be found online at https://doi.org/10.1016/j.geoderma.2024.116821.

References

Alexandre, A., Colin, F., Meunier, J-D., 1994. Les Phytolithes, indicateurs du cycle biogeochimique du silicium en forêt équatoriale. Comptes Rendus de l'Académie des Sciences de Paris. Série 2: Sciences de la Terre et des Planètes 319, 453-458.

Alexandre, A., Meunier, J.-D., Colin, F., Koud, J.-M., 1997. Plant impact on the biogeochemical cycle of silicon and related weathering processes. Geochim. Cosmochim. Acta 61 (3), 677–682.

Bartoli, F., 1985. Crystallochemistry and surface properties of biogenic opal. J. Soil Sci. 36 (3), 335–350.

Bartoli, F., Souchier, B., 1978. Cycle et rôle du silicium d'origine végétale dans les écosystèmes forestiers tempérés. Ann. Sci. For. 35 (3), 187–202.

Bartoli, F., Wilding, L.P., 1980. Dissolution of biogenic opal as a function of its physical and chemical properties. Soil Sci. Soc. Am. J. 44 (4), 873–878.

Blecker, S.W., McCulley, R.L., Chadwick, O.A., Kelly, E.F., 2006. Biologic cycling of silica across a grassland bioclimosequence. Global Biogeochem. Cycles 20 (3), GB3023.

Blum, W., Schad, P., Nortcliff, S., 2018. Essentials of soil science: Soil formation, functions, use and classification (World Reference Base, WRB). Schweizerbart, Stuttgart, Germany.

Brunauer, S., Emmett, P.H., Teller, E., 1938. Adsorption of gases in multimolecular layers. J. Am. Chem. Soc. 60 (2), 309–319.

Cabanes, D., Shahack-Gross, R., 2015. Understanding fossil phytolith preservation: the role of partial dissolution in paleoecology and archaeology. PLoS One 10 (5), e0125532.

Cabanes, D., Weiner, S., Shahack-Gross, R., 2011. Stability of phytoliths in the archaeological record: a dissolution study of modern and fossil phytoliths. Journal Archaeological Science 38 (9), 2480–2490.

Calegari, M.R., Madella, M., Vidal-Torrado, P., Otero, X.L., Macias, F., Osterrieth, M., 2013. Opal phytolith extraction in oxisols. Quat. Int. 287, 56–62.

de Tombeur, F., Turner, B.L., Laliberté, E., Lambers, H., Mahy, G., Faucon, M.-P., Zemunik, G., Cornelis, J.-T., 2020. Plants sustain the terrestrial silicon cycle during ecosystem retrogression. Science 369 (6508), 1245–1248.

Desplanques, V., Cary, L., Mouret, J.C., Trolard, F., Bourrié, G., Grauby, O., Meunier, J. D., 2006. Silicon transfers in a rice field in Camargue (France). J. Geochem. Explor. 88 (1), 190–193.

FAO, 1979. Soil map of the world (Vol. IX) Paris: UNESCO.

Fraysse, F., Pokrovsky, O.S., Schott, J., Meunier, J.-D., 2006. Surface properties, solubility and dissolution kinetics of bamboo phytoliths. Geochim. Cosmochim. Acta 70 (8), 1939–1951.

Fraysse, F., Pokrovsky, O.S., Schott, J., Meunier, J.-D., 2009. Surface chemistry and reactivity of plant phytoliths in aqueous solutions. Chem. Geol. 258 (3), 197–206.

Guntzer, F., Keller, C., Meunier, J.-D., 2012. Benefits of plant silicon for crops: a review. Agron. Sustain. Dev. 32 (1), 201–213.

Haysom, M.B.C., Chapman, L.S., 1975. Some aspects of the calciumsilicate trials at Mackay. Proc. Qls. Soc. Sug. Cane Technol. 42, 117–122.

Imaizumi, K., Yoshida, S., 1958. Edaphological studies on silicon supplying power of paddy fields.

ISO 13320, 2009: Particle size analysis – Laser diffraction methods. International Organization for Standardization (ISO).

ISO 11277, 2020. Soil Quality – Determination of Particle Size Distribution in Mineral Soil Material – Method by Sieving and Sedimentation. International Organization for Standardization (ISO).

IUSS Working Group WRB. 2022. World Reference Base for Soil Resources. International soil classification system for naming soils and creating legends for soil maps. 4th edition. International Union of Soil Sciences (IUSS), Vienna, Austria.

Klotzbücher, T., Marxen, A., Jahn, R., Vetterlein, D., 2016. Silicon cycle in rice paddy fields: insights provided by relations between silicon forms in topsoils and plant silicon uptake. Nutr. Cycl. Agroecosyst. 105 (2), 157–168.

Koebernick, N., Mikutta, R., Kaiser, K., Klotzbücher, A., Klotzbücher, T., 2022. Redox-dependent surface passivation reduces phytolith solubility. Geoderma 428, 116158.

Kögel-Knabner, I., Amelung, W., Cao, Z., Fiedler, S., Frenzel, P., Jahn, R., Kalbitz, K., Kölbl, A., Schloter, M., 2010. Biogeochemistry of paddy soils. Geoderma 157, 1–14.

Kraska, J.E., Breitenbeck, G.A., 2010. Survey of the silicon status of flooded rice in louisiana. Agron. J. 102 (2), 523–529.

Li, Z., Meunier, J.D., Delvaux, B., 2022. Aggregation reduces the release of bioavailable silicon from allophane and phytolith. Geochim. Cosmochim. Acta 325, 87–105.

Li, Z., Meunier, J.D., Delvaux, B., 2023. Goethite affects phytolith dissolution through clay particle aggregation and pH regulation. Geochim. Cosmochim. Acta 349, 11–22.

Liu, H., Meunier, J.D., Grauby, O., Labille, J., Alexandre, A., Barboni, D., 2023. Dissolution does not affect grass phytolith assemblages. Palaeogeogr. Palaeoclimatol. Palaeoecol. 610, 111345.

Marxen, A., Klotzbücher, T., Jahn, R., Kaiser, K., Nguyen, V., Schmidt, A., Schädler, M., Vetterlein, D., 2016. Interaction between silicon cycling and straw decomposition in a silicon deficient rice production system. Plant and Soil 398 (1–2), 153–163.

Mehra, O.P., Jackson, M.L., 1958. Iron oxide removal from soils and clays by a dithionite-citrate system buffered with sodium bicarbonate. Clay Clay Miner. 7, 317–327.

Nguyen, M.N., Dultz, S., Guggenberger, G., 2014. Effects of pretreatment and solution chemistry on solubility of rice-straw phytoliths. J. Plant Nutr. Soil Sci. 177 (3), 349–359.

Nguyen, M.N., Dultz, S., Picardal, F., Bui, A.T., Pham, Q.V., Dam, T.T., Nguyen, C.X., Nguyen, N.T., Bui, H.T., 2016. Simulation of silicon leaching from flooded rice paddy soils in the Red River Delta. Vietnam. Chemosphere 145 (45), 450–456.

Nguyen, M.N., Dultz, S., Meharg, A., Pham, Q.V., Hoang, A.N., Dam, T.T.N., Nguyen, V. T., Nguyen, K.M., Nguyen, H.X., Nguyen, N.T., 2019. Phytolith content in Vietnamese paddy soils in relation to soil properties. Geoderma 333, 200–213.

Nguyen, A.T.Q., Nguyen, A.M., Nguyen, L.N., Nguyen, H.X., Tran, T.M., Tran, P.D., Dultz, S., Nguyen, M.N., 2021. Effects of CO_2 and temperature on phytolith dissolution. Sci. Total Environ. 772, 145469.

Parr, J.F., Lentfer, C.J., Boyd, W.E., 2001. A comparative analysis of wet and dry ashing techniques for the extraction of phytoliths from plant material. J. Archaeol. Sci. 28 (8), 875–886.

Parr, J.F., Sullivan, L.A., 2005. Soil carbon sequestration in phytoliths. Soil Biol. Biochem. 37 (1), 117–124.

Peel, M.C., Finlayson, B.L., McMahon, T.A., 2007. Updated world map of the Köppen-Geiger climate classification. Hydrol. Earth Syst. Sci. 11 (5), 1633–1644.

Piperno, D.R., 2006. Phytoliths: a comprehensive guide for archaeologists and paleoecologists. Rowman Altamira, Lanham, USA.

R Core Team, 2021. A Language and Environment for Statistical Computing. The R Foundation for Statistical Computing.

Sahrawat, K., 2005. Fertility and organic matter in submerged rice soils. Curr. Sci. 88 (5), 735–739.

Sauer, D., Saccone, L., Conley, D., Herrmann, L., Sommer, M., 2006. Review of methodologies for extracting plant-available and amorphous Si from soils and aquatic sediments. Biogeochemistry 80, 89–108.

Savant, N.K., Datnoff, L.E., Snyder, G.H., 1997. Depletion of plant-available silicon in soils: a possible cause of declining rice yields. Commun. Soil Sci. Plant Anal. 28 (13–14), 1245–1252.

Schwertmann, U., 1964. Differenzierung der Eisenoxide des Bodens durch Extraktion mit Ammoniumoxalat-Lösung. Zeitschrift Für Pflanzenernährung, Düngung, Bodenkunde 105 (3), 194–202.

Sze, A., Erickson, D., Ren, L., Li, D., 2003. Zeta-potential measurement using the Smoluchowski equation and the slope of the current–time relationship in electroosmotic flow. J. Colloid Interface Sci. 261 (2), 402–410.

Tsujimoto, Y., Muranaka, S., Saito, K., Asai, H., 2014. Limited Si-nutrient status of rice plants in relation to plant-available Si of soils, nitrogen fertilizer application, and rice-growing environments across Sub-Saharan Africa. Field Crop Res 155, 1–9.

Vander Linden, C., Li, Z., Iserentant, A., Van Ranst, E., de Tombeur, F., Delvaux, B., 2021. Rainfall is the major driver of plant Si availability in perudic gibbsitic Andosols. Geoderma 404, 115295.

Vandevenne, F., Struyf, E., Clymans, W., Meire, P., 2012. Agricultural silica harvest: have humans created a new loop in the global silica cycle? Front. Ecol. Environ. 10 (5), 243–248.

White, A.F., Brantley, S.L., 2003. The effect of time on the weathering of silicate minerals: why do weathering rates differ in the laboratory and field? Chem. Geol. 202 (3), 479–506.

Wickramasinghe, D.B., Rowell, D.L., 2006. The release of silicon from amorphous silica and rice straw in Sri Lankan soils. Biol. Fertil. Soils 42 (3), 231–240.

Yang, X., Song, Z., Qin, Z., Wu, L., Yin, L., Van Zwieten, L., Song, A., Ran, X., Yu, C., Wang, H., 2020. Phytolith-rich straw application and groundwater table management over 36 years affect the soil-plant silicon cycle of a paddy field. Plant and Soil 454 (1), 343–358.